









Inertia Estimation of a Power System Area Based on Iterative Equation Error System Identification

Davide Gotti , *Member, IEEE*, Federico Bizzarri , *Senior Member, IEEE*,
Angelo Brambilla , *Senior Member, IEEE*, Davide del Giudice , *Member, IEEE*,
Samuele Grillo , *Senior Member, IEEE*, Daniele Linaro , *Member, IEEE*, Pablo Ledesma ,
and Hortensia Amaris , *Senior Member, IEEE*

Abstract—This paper proposes an area inertia estimator based on an iterative equation error (EE) system identification (SI) approach. The inertia value can be accurately extracted for areas of different compositions with different penetrations of converter-interfaced generators. Firstly, the internal frequency variation of the generator units is computed by means of a frequency divider-based estimator. Subsequently, these internal frequency variations are used to carry out a generator clustering, which provides groups of coherent generators to the proposed inertia estimator. Finally, the iterative EE SI approach provides a joint inertia estimation for each of these coherent groups. Numerical results on a properly modified version of both the IEEE 39-bus and the IEEE 118-bus test systems highlight the accuracy of the proposed method using both ambient measurements and ringdown signal measurements (power imbalance events). Furthermore, the proposed method presents a low computational burden that allows fast estimation updating times.

Index Terms—Area inertia estimation, system identification, converter-interfaced generator, synchronous generator, generator clustering.

I. INTRODUCTION

A. Motivation

THE growing integration of converter-interfaced generators (CIGs) installed in power systems during recent years poses new challenges for transmission system operators

Manuscript received 24 May 2023; revised 11 November 2023; accepted 4 January 2024. Date of publication 11 January 2024; date of current version 21 August 2024. This work was supported by Agencia Estatal de Investigación MCIN/AEI/ 10.13039/501100011033 under Grant PID2019-104449RB-I00. Paper no. TPWRS-00791-2023. (*Corresponding author: Davide Gotti.*)

Davide Gotti, Pablo Ledesma, and Hortensia Amaris are with the Department of Electrical Engineering, Universidad Carlos III de Madrid, 28911 Madrid, Spain (e-mail: dgotti@ing.uc3m.es; pablole@ing.uc3m.es; hortensia.amaris@uc3m.es).

Federico Bizzarri is with the Dipartimento di Elettronica, Informazione e Bioingegneria, Politecnico di Milano, 20133 Milano, Italy, and also with the Advanced Research Center on Electronic Systems for Information and Communication Technologies E. De Castro (ARCES), University of Bologna, 41026 Bologna, Italy (e-mail: federico.bizzarri@polimi.it).

Angelo Brambilla, Davide del Giudice, Samuele Grillo, and Daniele Linaro are with the Dipartimento di Elettronica, Informazione e Bioingegneria, Politecnico di Milano, 20133 Milano, Italy (e-mail: angelo.brambilla@polimi.it; davide.delgiudice@polimi.it; samuele.grillo@polimi.it; daniele.linaro@polimi.it).

Color versions of one or more figures in this article are available at <https://doi.org/10.1109/TPWRS.2024.3353077>.

Digital Object Identifier 10.1109/TPWRS.2024.3353077

(TSOs) [1]. One of the most important concerns is the variability of the inertia provided by CIGs, which can be easily changed by acting on their control system, potentially leading to the formation of areas with low inertia. This could be a problem since reduced inertia may lead to a high rate of change of frequency (RoCoF) that could trigger frequency relay protections and, in turn, provoke frequency stability issues. In this regard, it is worth mentioning that a recent technical report from the European Network of Transmission System Operators considers the decrease of inertia as the top concern among power-system-related challenges [2]. In light of these considerations, this article proposes an area inertia estimator capable of providing accurate estimates considering the presence of CIGs and exploiting both ambient and ringdown (power imbalance events) signal measurements.

B. Literature Review

In recent years, a large number of inertia estimation algorithms have been proposed. Some of them focus on single devices, whereas others focus on area-wide applications. In the first case, the inertia of a single generator is estimated, whereas in the latter the inertia of an area possibly comprising more than one generator is estimated. Regardless of the scope, most of those methods exploit the information received from ringdown signal measurements, although some works have recently made use of ambient signals. A detailed review of recently proposed inertia estimators can be found in [3], [4], [5].

Among the recently proposed algorithms focused on the single-device inertia estimation, [6] introduces a new index called the rate of change of power (RoCoP) that can be used to estimate the inertia of single devices, and it is applicable for both synchronous generators (SGs) and CIGs. Results suffer from numerical oscillations - a problem addressed in [7] by converting algebraic equations into first-order differential equations. However, reported results are obtained supposing sampling times of 1 ms, whereas phasor measurement units (PMUs) can achieve sampling times on the order of tens of frames per second [8]. An adaptive unscented Kalman filter to estimate the inertia of SGs is proposed in [9]. Simulations provide accurate results and very quick convergence times; however, only short-circuit events are considered and the method is not applicable to CIGs. An extension is proposed by the authors in [10] where the inertia estimation of CIGs is addressed, but the algorithm is not tested

under normal operating conditions. Reference [11] points out that the covariance of voltage and current ambient measurements is related to the inertia values of SGs and CIGs, and solves a least-square problem to fit the measurements to the generation unit models. However, a systematic method to find the optimal location of PMUs to gather the ambient measurements still needs to be found. A data-driven inertia estimator applicable to both SGs and CIGs is proposed in [12]. Reported results are accurate and robust to high noise levels. However, this approach requires the TSO to have access to the internal frequency and internal angles of the generation units, which are not always available.

Regarding recent works with an area-wide scope, reference [13] proposes an autoregressive moving average with exogenous inputs (ARMAX)-based method to estimate the effective inertia of a power system. The electrical frequency of some buses measured by PMUs is used as input for the ARMAX system identification process, but no indication regarding the selection of these buses is given. In [14], a dynamic regressor extension and mixing technique is used to estimate the inertia of a power system. This work does not consider the inertial contribution from CIGs and was tested only under significant power imbalance conditions like power plant outages. A power system inertia estimation algorithm based on the RoCoF estimation is proposed in [15]. Reported results are accurate, but this method does not consider the presence of CIGs and requires knowing the magnitude and the occurrence time of the power imbalance event. A methodology to estimate separately the aggregated inertial response of SGs, of CIGs, along with the inertial contribution of loads is proposed in [16]. Provided results are accurate, but this method is not applicable under normal operating conditions and it requires that the TSO knows the magnitude of the power imbalance and the share of loads with a frequency-independent behavior connected in the system at the time of the event—a piece of information not always available [5]. In [17], an area inertia estimation is carried out by analyzing the electromechanical oscillations response in the frequency domain of an equivalent SG that represents an area. However, the methodology is applicable only to areas that contain SGs and approximates the frequency of the area by taking frequency measurements at a representative bus, an assumption that may lead to large errors [1]. Reference [18] proposes a method to estimate the inertia of a sub-network by using reactive power measurements. The method provides accurate estimations only under relatively small power imbalances and is not tested under normal operating conditions.

C. Contributions

This article proposes a system identification (SI) based estimator able to provide estimates of the inertia of areas. It only requires the knowledge of the set of generators that compose an area and the measurement of the active power and the bus frequency taken at the generation buses, which are easily obtained by a PMU at each power plant substation. The main contributions of this article are the following:

- An algorithm that is able to provide the inertia of areas composed entirely of SGs, CIGs, or mixed areas with

different penetration of CIGs. The algorithm is also able to provide accurate inertia estimates of single devices.

- The article also provides a simple yet effective method to cluster generators that have coherent electromechanical oscillations after power imbalance events.
- Unlike other works in literature, the proposed method can provide inertia estimates both under normal operating conditions and after a power imbalance event. Furthermore, it does not require any knowledge regarding the location and the entity of the power imbalance events.
- The methodology can be used in real-time operation since it requires observation windows of a few minutes when the system is under normal operating conditions and of a few tens of seconds after a power imbalance event.

II. DESCRIPTION OF THE ALGORITHMS

A. Iterative Equation Error Model

System identification methods can be used to estimate the parameters of a transfer function if its input and output signals are known [19]. The equation error (EE) model is one of the most common model structures due to its low computational burden and stability properties. The EE model structure can be derived considering the following input-output relationship described as a linear difference equation:

$$\begin{aligned} y(t) + a_1y(t-1) + a_2y(t-2) + \dots + a_{n_a}y(t-n_a) = \\ = b_1u(t-1) + b_2u(t-2) + \dots + b_{n_b}u(t-n_b) + e(t), \end{aligned} \quad (1)$$

where $y(t)$ is the output signal, $u(t)$ is the input signal, and n_b and n_a are the numerator and denominator order, respectively. The EE model formulation takes its name after the presence of the white noise $e(t)$ that acts as an error and is directly entered in the difference equation.

By defining the following parameter vector:

$$\theta = [b_1, b_2, \dots, b_{n_b}, a_1, a_2, \dots, a_{n_a}]^T, \quad (2)$$

and the following information vector:

$$\varphi(t) = [u(t-1), \dots, u(t-n_b), -y(t-1), \dots, -y(t-n_a)]^T, \quad (3)$$

it is possible to derive the one-step-ahead predictor:

$$\hat{y}(t) = \varphi(t)^T \theta. \quad (4)$$

This linear regression allows the one-step-ahead prediction of the output signal by knowing the parameter vector and the information vector (which includes only past measurements). However, this formulation can also be used to derive the parameter vector using an iterative formulation so that the predicted output $\hat{y}(t)$ fits as best as possible the measured output signal $y(t)$. In fact, by considering the stacked output vector $\mathbf{Y}(L) = [y(L), y(L-1), \dots, y(1)]^T$ and the stacked information matrix $\mathbf{\Phi}(L) = [\varphi(L), \varphi(L-1), \dots, \varphi(1)]^T$, both over the L elements of the data batch, and applying the least square formulation:

$$\theta = (\mathbf{\Phi}^T \mathbf{\Phi})^{-1} \mathbf{\Phi}^T \mathbf{Y}, \quad (5)$$

it is possible to determine the parameter vector. Since the process is carried out considering a data batch with finite length L , this method falls under the so-called iterative formulation [19], hence the name iterative EE model. Once the parameter vector has been computed, the discrete-time z domain transfer function can be computed as:

$$H(z) = \frac{z^{n_a - n_b} b_0 z^{n_b} + b_1 z^{n_b - 1} + \dots + b_{n_b - 1} z + b_{n_b}}{z^{n_a} + a_1 z^{n_a - 1} + \dots + a_{n_a - 1} z + a_{n_a}} \quad (6)$$

Compared to other models, the EE has the advantage of providing a solution that is guaranteed to be the global minimum, since the parameter vector is a quadratic function of the information vector. The interested reader can refer to [19] and [20] for a more in-depth discussion on these topics.

B. SG/CIG Transfer Function and Their Z-Domain Equivalent

Let us consider the electromechanical swing equation of the SG, which represents the dynamics of the rotor [21]:

$$M_g \frac{d\Delta\omega_g}{dt} = \Delta P_m - \Delta P_g - D\Delta\omega_g, \quad (7)$$

where $\Delta\omega_g$ represents the internal frequency variations of the SG, ΔP_m is the variation of the mechanical power, ΔP_g represents the variation of the power supplied to the network by the generator, D is the load-damping coefficient, and M_g ¹ is the mechanical time constant of the SG inertia, which is twice the inertia constant H_g . P_m includes the following terms:

$$P_m = P_{UC} + P_{PFC} + P_{AGC}. \quad (8)$$

P_{UC} is the power set point determined through the unit commitment problem, which is piece-wise constant and, thus, such that $\Delta P_{UC} = 0$. P_{AGC} is the active power provided by the automatic generation control (AGC), if present. The AGC presents slow activation times after power imbalance events and does not activate when the system is under normal operating conditions. In the time scales of this work, its variations can be safely neglected. P_{PFC} represents the active power produced by the primary frequency control (PFC), whose variations ΔP_{PFC} are not negligible since they play a significant role in the response of the generator during the first seconds after a perturbation. Thus, it can be assumed that:

$$\Delta P_m \approx \Delta P_{PFC}. \quad (9)$$

The active power variation due to PFC can be represented by the following expression in the s -domain:

$$\Delta P_{PFC} = -\frac{R^{-1}}{1 + sT} \Delta\omega_g, \quad (10)$$

where R is the PFC droop gain and T is an equivalent time constant of the PFC control system that represents governor and turbine dynamics with a single time delay block. It is worth noticing that with this simplified model, composed of a gain and a time delay, it is not possible to detect the internal dynamics of the turbine and governor. However, this is of little importance since this work focuses on the estimation of M_g .

Taking the Laplace transform of (7) and including (10), the s -domain transfer function of an SG with PFC becomes:

$$\frac{\Delta\omega_g(s)}{\Delta P_g(s)} = -\frac{s \frac{1}{M_g} + \frac{1}{TM_g}}{s^2 + s \left(\frac{1}{T} + \frac{D}{M_g} \right) + \frac{D+R^{-1}}{TM_g}}, \quad (11)$$

Similarly, one can derive the transfer function of an SG that does not include the PFC:

$$\frac{\Delta\omega_g(s)}{\Delta P_g(s)} = -\frac{\frac{1}{M_g}}{s + \frac{D}{M_g}}. \quad (12)$$

Consider now the virtual swing equation of a CIG with a virtual synchronous machine (VSM) grid-forming control [22]:

$$M_{CIG} \frac{d\Delta\omega_{CIG}}{dt} = \Delta P_m - \Delta P_{CIG} - (k_w + k_D)\Delta\omega_{CIG}, \quad (13)$$

where M_{CIG} is the synthetic mechanical time constant, k_w and k_D are the inverse of the steady-state PFC droop gain and the damping constant, respectively, both provided by the VSM control system. Since both the PFC and the damping service are proportional to the internal frequency variation $\Delta\omega_{CIG}$, their effect can be included in a single parameter $G = k_w + k_D$.

Like in the previous case, by noticing that $\Delta P_m = \Delta P_{UC} + \Delta P_{AGC} \approx 0$ and doing the Laplace transform of (13), one gets:

$$\frac{\Delta\omega_{CIG}(s)}{\Delta P_{CIG}(s)} = -\frac{\frac{1}{M_{CIG}}}{s + \frac{G}{M_{CIG}}}. \quad (14)$$

It is worth noting that the transfer function representing the electromechanical oscillations of an SG equipped with PFC has two poles and one zero (11), while that of an SG without PFC and of a CIG with VSM control both present only one pole, as shown in (12) and in (14), respectively.

As detailed in the previous subsection, the EE model provides the parameters of a transfer function defined in the z -domain with given numerator and denominator orders. A transfer function with one pole and no zeros, e.g. (14) representative of CIGs or (11) referring to SGs without PFC, has the following general s -domain expression:

$$F(s) = \frac{num}{s + den}, \quad (15)$$

where num and den are generic numerator and denominator terms, respectively. Observing that (15) has the following equivalent z -domain expression [23]:

$$F(z) = \frac{z}{z - e^{-denT_s}}, \quad (16)$$

with T_s being the sampling period, and by comparing (6) with (16), it is possible to notice that $a_1 = e^{-denT_s}$ and $b_0 = -numT_s$ [23], where the parameters of a_1 and b_0 can be determined by applying the iterative EE SI method with denominator order $n_a = 1$ and numerator order $n_b = 1$. Finally, by comparing (15) with (14) and noticing that $num = \frac{1}{M_{CIG}}$ and $den = \frac{G}{M_{CIG}}$, one gets:

$$M_{CIG} = -\frac{1}{b_0} T_s, \quad ; \quad G = \frac{-\ln(a_1)}{T_s} M_{CIG} T_s \quad (17)$$

¹With a little abuse of notation, we refer from hereon to M_g as *inertia*.

Since this work focuses on the estimation of the inertia parameter, the expression on the right is not used further here. However, its application has been recently shown in [24].

A transfer function with two poles and one zero, representing an SG with PFC, can be written in the s -domain as

$$\frac{\Delta\omega_g(s)}{\Delta P_g(s)} = -\frac{s n_1 + n_2}{(s + d_1)^2 + d_2}, \quad (18)$$

where n_1, n_2, d_1 , and d_2 are generic numerator and denominator terms. The equivalent z -domain transfer function of (18) can be expressed as follows [23]:

$$F(z) = \frac{z^2 n_1 - z[n_1 e^{-cT_s} \cos(d_2 T_s) - \frac{n_2 - d_1 n_1}{d_2} \sin(d_2 T_s)]}{z^2 - 2z e^{-d_1 T_s} \cos(d_2 T_s) + e^{-d_1 T_s}}. \quad (19)$$

Similarly, by comparing (6) with (19) it is possible to observe that $b_0 = -n_1 T_s$. Finally, by comparing (18) with (11) it is easy to derive that $n_1 = \frac{1}{M_g}$, which leads to:

$$M_g = -\frac{1}{b_0} T_s, \quad (20)$$

where b_0 refers to the general formulation (6) and is provided by an iterative EE model with $n_a = 2$ and $n_b = 2$. By having also the other parameters of the z -domain transfer function, it is possible to determine the PFC droop gain, the load-damping coefficient D , and the equivalent time constant T . However, since this work focuses on estimating the inertia of areas, only this parameter is estimated.

C. Generator Clustering

As described later in Section III, the iterative EE model used to estimate the inertia of single devices can be profitably extended to area-wide applications provided that generators show similar electromechanical oscillations. Generally, generators in the same area are electrically near and thus present similar oscillations. However, if a significant power imbalance event occurs near or inside the area, generators may oscillate non-coherently with each other. In this case, the joint inertia estimation explained in Section III may be inaccurate.

To avoid this problem, a generator clustering method is proposed: it consists in grouping together generators with similar internal frequency oscillations so that their measurements can be merged to carry out a joint inertia estimation. Thus, this problem falls under the curve clustering topic. A comprehensive literature review on this topic, along with a new taxonomy on clustering approaches, is proposed in [25]. One of the most commonly used algorithms for curve classification is the k-means. However, these algorithms did not prove particularly useful in this work since the final result depends on cluster initialization, which is one of the drawbacks of the traditional k-means method that has not been fully solved by algorithm variants [26]. To get reproducible results, it would be necessary to solve several tens of classifications and take the most common output. However, this would increase the central processing unit (CPU) burden of the algorithm, compromising its online applicability. Furthermore, we noticed that the k-means tend to create more clusters

than necessary, thus separating generators that could be merged without compromising the area estimation accuracy.

Thus, in this work, a raw-data clustering approach [25] is used, which exploits the observational points of the curve and does not use dimensional-reduction techniques. The proposed method makes use of the root mean square (RMS) of the internal frequency variation differences between generators (determined with a frequency divider-based estimator) to carry out the clustering. This metric is computed separately for all the generators of the same area, and is determined as:

$$\Psi_{Gen_x, Gen_y} = \sqrt{\frac{1}{T} \sum_{t=1}^T [\Delta\omega_{Gen_x} - \Delta\omega_{Gen_y}]^2} \quad (21)$$

where Gen_x and Gen_y are two generation units (SGs or CIGs) of the same area, and $\Delta\omega_{Gen_x}$ and $\Delta\omega_{Gen_y}$ are their internal frequency variations. The clustering RMS metric is computed over the first few seconds of the simulation after power imbalance events. In fact, this period is sufficient to detect different electromechanical oscillations and separate non-coherent generators. Once all the mutual RMS distances related to an area have been computed, a threshold $\Psi_{threshold}$ is used to determine if the generators are to be clustered together or not. How to choose this clustering threshold is empiric, and it depends on the electric network under study and on the considered time span (21). In this regard, it is worth noticing that by adopting different observation times T the RMS of the internal frequency differences will vary. Thus, $\Psi_{threshold}$ should be selected accordingly. This selection follows a trial-and-error approach. To avoid unnecessary clustering, some simulations must be carried out to verify that the clustering method is not too sensitive. At the same time, its responsiveness must be assessed to guarantee that the input and output signals used by the proposed SI can be properly merged without jeopardizing estimation accuracy. However, as shown in Section IV, tuning $\Psi_{threshold}$ is rather simple.

To be clustered together, all generators must have mutual RMS metrics lower than $\Psi_{threshold}$. Despite its simplicity, this method is very effective in grouping generators with coherent electromechanical oscillations and allows the proposed area inertia estimator to provide accurate estimates. Moreover, the CPU times needed to perform this clustering range from a few ms to a few tens of ms, based on the number of generators to be grouped and the final number of sub-groups.

III. IMPLEMENTATION

Fig. 1 summarizes the method proposed in this work, which resorts to an iterative EE SI algorithm to carry out the inertia estimation of areas. As described in Section II, the iterative EE model allows one to estimate the parameters of a transfer function by measuring its input and output signals. In our case, the input signal is the active power variation, whereas the output signal is the internal frequency variation, as shown in (11), (12), and (14). Since the latter may not be accessible to the TSO, in this work it is estimated by using the model-independent internal frequency estimator proposed in [27], which only needs bus frequency measurements (denoted by Δf_i in Fig. 1) taken at

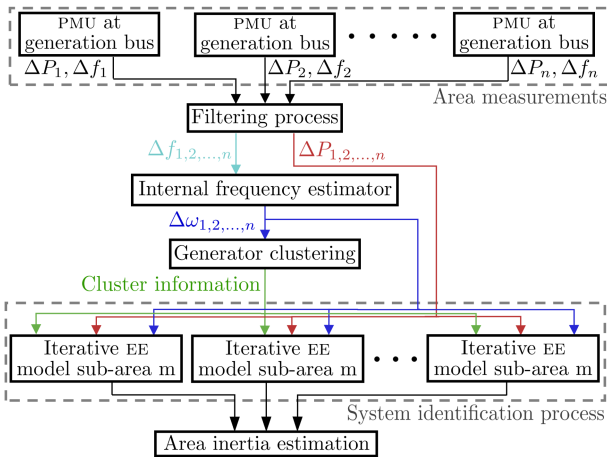


Fig. 1. Flowchart of the proposed method.

the power plant substation. However, other methods such as that proposed in [9] can be used for this purpose. It should be noted that the proposed algorithm only requires installing PMUs at the power plant substations to estimate the inertia of areas.

As indicated in [19], SI methods benefit from signal filtering because the presence of the noise may reduce their accuracy. Therefore, a low-pass filter is applied to both the active power and the bus frequency measurements.

Since the ultimate goal of this work is to estimate the inertia of areas, the proposed approach carries out a joint estimation for every generation unit that is in the analyzed area. In particular, the active power variations of all generation units are added to get an equivalent input signal, and an average value of the internal frequency variations is carried out to compute the equivalent output signal. Subsequently, these two signals are used to carry out a parameter estimation of an equivalent transfer function of the area, i.e., a joint inertia estimation of every generation unit is made.

To provide accurate inertia estimates of areas by using an equivalent transfer function, the generators must have coherent electromechanical oscillations. Otherwise, using the average value of the internal frequency variations of all the devices may not give a significant equivalent average frequency variation of the area. This is not a problem when the system is under normal operating conditions since the internal frequency of the generation units of an area experiences similar oscillations. However, power imbalance events may cause generators pertaining to the same geographical area to oscillate differently. Therefore, carrying out a joint inertia estimation by considering their input and output signals together may lead to large estimation errors. To avoid this inconvenience, the generator clustering method is used. Once the generators with similar electromechanical oscillations are grouped together, the equivalent input and output signals of the sub-areas are computed and their inertia values are estimated.

In this regard, it is worth mentioning that the areas of the electric network are first determined by analyzing the system under normal operating conditions. In fact, if the generators present similar internal frequency variations under this condition, they

can be grouped together and accurate inertia estimations can be obtained. This first partitioning is intended to define fixed areas with a geographical meaning since, generally, generation units with small electrical distances present similar oscillations. Then, the clustering method is applied to each area to verify that its generators are coherent with each other after power imbalance events. If any incoherency is identified, the proposed clustering method provides sub-groups of coherent generators whose inertia is estimated separately. After this process, these inertia values are summed to obtain the inertia of the area. So doing, the TSO can estimate the inertia of the zones it is interested in monitoring even if their generators oscillate differently following a perturbation. Thus, this method presents the advantage of providing the inertia value of a geographically defined area, even if during a power imbalance event this area includes non-coherent generators.

The proposed method is applicable to both SGs and CIGs. As shown in subsection II-B, the transfer function of an SG with PFC has two poles and one zero, whereas the CIG transfer function has one pole. Therefore, an area that has only SGs with PFC will have an equivalent transfer function of the second order, and the iterative EE SI will be tuned accordingly to estimate the parameters of a transfer function with this shape. Similarly, an area composed only of CIGs will have an equivalent transfer function of the first order. If an area includes both SGs and CIGs, the order of the transfer function that best fits the equivalent dynamic behavior of the area has to be found. As detailed later in Section IV, this is not a limiting factor since the determination of the order of the equivalent transfer function that provides good estimates is not difficult.

IV. TEST RESULTS

This section discusses the estimation accuracy of the proposed algorithm and its compatibility with both ambient measurements and ringdown signals (power imbalance events). The first and second subsections respectively present estimation results on the IEEE 39-bus and 118-bus test systems, which were both modified by replacing several SGs with CIGs; the parameters of the CIGs used in this work are listed in [28]. Simulations are carried out using the software DiGSILENT PowerFactory. SGs are modeled by using either round rotor models with one damper winding in the d-axis and two damper windings in the q-axis, or salient pole models with one damper winding in both the d- and q-axis. It is important to remark that even if the system identification method is applied to the simplified swing equation of SGs (11), the simulations are carried out by using complete models of SGs. Thus, the simplifications described in Section II do not limit the generality of the proposed approach. CIG plants and their VSM control system are modeled as indicated in [29].

To represent the frequency oscillations that characterize power systems under normal operating conditions, the power consumption of loads is modeled by an Ornstein-Uhlenbeck (OU) stochastic process [30]. The OU process of loads is characterized by a standard deviation of 1% of the load nominal power, and an autocorrelation coefficient of 0.5 Hz. Both the active and the reactive power consumption are perturbed using two

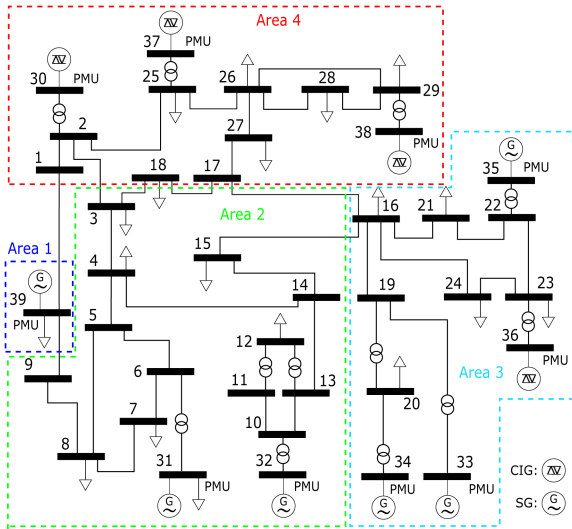


Fig. 2. Single-line diagram (with areas) of the IEEE 39-bus test system.

uncorrelated processes. We assume that the loads of the IEEE 39- and 118-bus test systems are aggregated models of uncorrelated much smaller ones that contribute to the same buses. This leads to our choice of the standard deviation and of the autocorrelation values, which are in agreement with those reported in previous works [31], [32], [33], [34]. However, in this section, to verify the generality of the proposed method, several tests considering different autocorrelation values of the OU stochastic process are carried out. Besides, a normal Gaussian distributed noise as described in [35] is applied for both bus frequency and active power measurements.

The area inertia estimator based on the iterative EE SI approach is coded in MATLAB and makes use of the bus frequency and active power measurements imported from PowerFactory. Measurements are exported using a sampling time of 10 ms, which can be easily achieved by commercially available PMUs [8]. All measurements are filtered using the *lowpass* function of MATLAB, with a cutoff frequency of 2 Hz. The inertia values reported in this section are referred to 100 MVA, which is the reference power of the network. The PC used to carry out the tests is an Intel Core i7-1255 U 1.7 GHz, equipped with 16 GB of RAM.

A. Test Results on IEEE-39 Bus Test System

This test system has been modified by substituting traditional SGs at buses 30, 36, 37, and 38 with CIGs of the same apparent power. As it can be observed in Fig. 2, the system is divided into 4 different areas. Area 1 is constituted only by the SG connected to bus 39, which represents the upstream US and Canadian network, and is modeled without any control systems such as automatic voltage regulator (AVR), governor, and power system stabilizer (PSS). Area 2 is constituted by SG 31 and SG 32 (from hereafter, SGs and CIGs are labeled after the bus number they are connected to). Area 3 has SG 33, SG 34, SG 35, and CIG 36; therefore, it presents a mixed composition. Area 4 includes CIG 30, CIG 37, and CIG 38. The values of the inertia of the

TABLE I
IEEE-39 BUS SYSTEM—AREA COMPOSITION AND INERTIA VALUES

	Area 1	Area 2	Area 3	Area 4
Area composition	SG 39	SGs 31/32	SGs 33/34/35 CIG 36	CIGs 30/37/38
Equivalent transfer function	1 pole	2 poles, 1 zero	2 poles, 1 zero	1 pole
SG-CIG M (MWs/MVA)	1000	60.6/71.6	57.2/52/69.6 56	70/56/65
Area M (MWs/MVA)	1000	132.2	234.8	191

single generation units and of the areas are reported in Table I. In accordance with the considerations made in Section III, areas 1 and 4 are modeled by first-order transfer functions, with one pole and no zeros. Area 2, composed only of SGs, is modeled by a second-order transfer function, with two poles and one zero. Although Area 3 does not contain only SGs, the results show that a second-order transfer function provides accurate results under both normal operating conditions and power imbalance events.

Generally, generators that are electrically near each other present similar electromechanical oscillations and, thus, can be grouped together by using the proposed SI approach. Specifically, areas are determined through several inertia estimations using ambient measurements and by verifying that their joint inertia estimation is accurate. However, it is worth highlighting that the composition of the area is empirical and more than one possible composition may exist, especially in large and meshed systems where areas are not often well-defined.

1) *Normal Operating Conditions*: In this case study, the system is under normal operating conditions, i.e., only the stochastic process of loads is considered and no other power imbalance event is simulated. Therefore, the estimation is carried out by using ambient measurements. The iterative EE SI approach is used to estimate the inertia of the 4 areas composed as described earlier. Observation windows of 5, 3, and 1-minute durations are tested. To create a statistically representative simulation batch, a 6-hour-long simulation is carried out. Therefore, in the case of the 5-minute-long window, 72 independent simulations are carried out. On the contrary, for 3 and 1-minute-long observation windows, 120 independent estimations are executed. The observation windows used in this result section correspond to the data batch of L elements described in subsection II-A. For instance, since we use a sampling time of 10 ms, the 5-minute-long observation window used in this work is composed of $L = 30\,000$ samples. Estimation results are reported in Fig. 3 in the form of violin plots, where the horizontal bar represents the mean estimation value, the black rectangle shows the ends of the first and third quartiles of the data, and the vertical black line connects the ends of the upper and the lower adjacent values (smallest/highest values within the third/first quartile plus/minus 1.5 times the inter-quartile range, respectively). To easily compare area estimates, results are normalized with respect to the actual M values shown in Table I. Thus, the closer the mean value to 1 p.u. and the smaller the bandwidth of the violin plot, the more accurate and reliable the estimations.

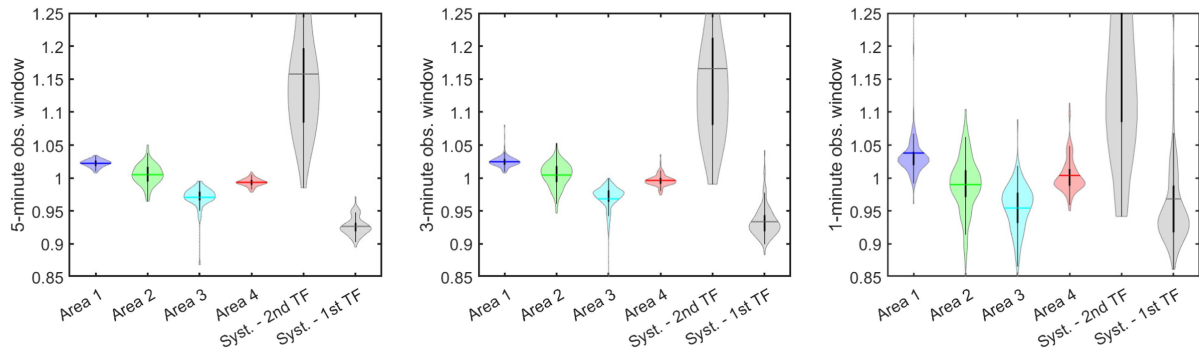


Fig. 3. IEEE-39 bus system—Violin plots of the normalized M estimates with 5-, 3-, and 1-minute-long observation windows using ambient measurements.

As expected, the wider the observation window, the better the estimates provided by the proposed iterative EE SI. In terms of mean values, the difference between different observation windows is appreciable but not substantial. However, wider observation windows allow for more reliable estimations since their probability distribution is shorter. This comes with the drawback of a slower estimation update, as shown in the next subsection. Both the 5 and 3 minute-long observation windows provide very accurate estimates with average errors generally below 3% and relatively limited maximum errors. Although the 1 minute-long observation window has slightly higher average estimation errors, its estimations are affected by sensibly higher maximum errors. Thus, we advocate using this observation window only if the TSO needs a quick estimation update and high precision is not an important issue.

It should be noted that the inertia estimation of the whole system, obtained by grouping the measurements of all 10 generation units, is not as precise as the estimation of areas analyzed separately. Indeed, as shown by the two rightmost violin plots in each panel of Fig. 3, by supposing an equivalent transfer function of the first and second order for the entire system and applying the proposed method, the M estimation errors are sensibly higher compared to ones of the areas. The rationale behind this is that the generation units experience coherent electromechanical oscillations if they are electrically near. Otherwise, even if the system is under normal operating conditions, these oscillations are not sufficiently similar to group together all the generators, leading to worse estimates. From this consideration, it is clear that the proposed method works better if applied to areas instead of entire systems.

2) *Time-Varying Inertia Under Normal Operating Conditions*: One of the most important features of our proposed estimator is the capability to track changes of inertia over time just by using ambient measurements. Since the inertia of SGs is a constant value, to test the capability of the proposed method to detect time-varying inertia we act on the control of CIGs. In particular, we change the control setting of the generation units of area 4. Initially, the inertia value of the area is 191 MWs/MVA, as represented in Table I. The simulation lasts 20 minutes and only the stochastic process of loads is considered. After 6 minutes of simulation, we reduce by 50% the synthetic inertia provided by CIG 30, CIG 37, and CIG 38, obtaining an

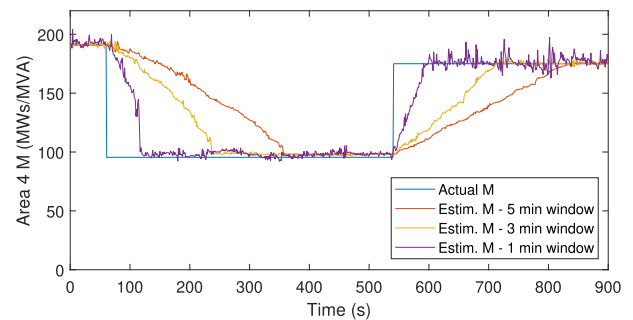


Fig. 4. IEEE 39-bus system—Time-varying M detected by ambient measurements.

actual inertia value of area 4 of 95.5 MWs/MVA. This value is maintained for 8 minutes, i.e., until the simulation time reaches 14 minutes. At this point, CIG 30 and CIG 38 restore the inertia they provide to the initial value, whereas CIG 37 provides an inertia value of 40 MWs/MVA. Therefore, at the end of the simulation, the inertia of area 4 is 175 MWs/MVA.

To track these changes, we opt for an observation window with a 1 s time offset, i.e., the observation window allows the proposed estimator to update its estimation every 1 s. It is worth pointing out that the CPU time of one estimation using the proposed iterative EE SI estimator with a 5-minute observation window is about 10 ms, well below the time offset of 1 s. Thus, the algorithm can be applied in real-time since it is sufficiently fast to update the estimates after a new observation window has to be analyzed.

Fig. 4 depicts the estimates using 5, 3, and 1 minute-long observation windows. Fig. 4 only represents 15 minutes of the simulation because the first 5 minutes are used by the observation window to provide the first estimate. After that, the values are updated every second. It can be noticed that the wider the observation window, the smaller the oscillations around the actual value. This is coherent with the considerations related to Fig. 3, where wider observation windows presented lower average and maximum errors compared to narrower windows. However, it is possible to observe how narrower windows allow faster detection of inertia changes. Particularly, a 5-minute length window needs approximately 5 minutes to fully detect the inertia changes, which is the time required for the observation

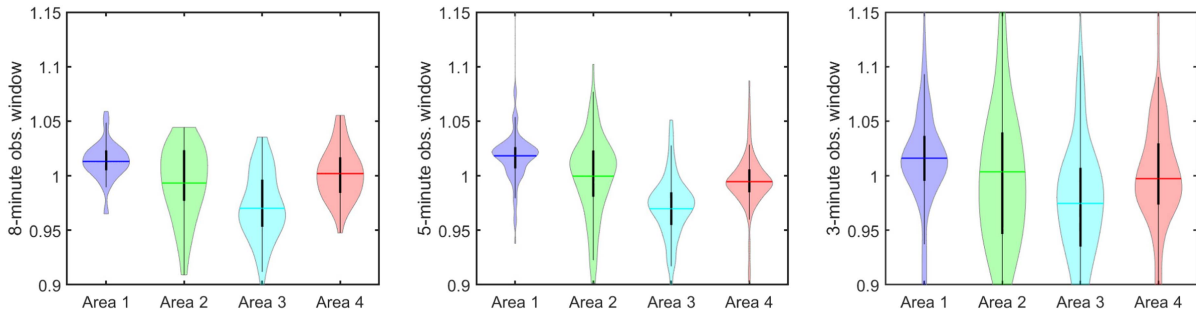


Fig. 5. IEEE-39 bus system (OU process with autocorrelation of 0.01 Hz)—Violin plots of the normalized M estimates with 8-, 5-, and 3-minute-long observation windows.

window to include only ambient measurements that are related to new inertia values. Obviously, a 1 minute-long observation window allows a faster discounting of measurements related to old conditions, but this comes with the price of higher oscillations. As previously commented, the TSO should consider whether very precise estimations or fast-tracking behavior are needed and decide the window length that best suits the specific application under study. One possible solution may be the application of several window lengths in parallel to combine the benefits of very accurate estimates and faster updating times.

3) *Effect of the Autocorrelation Coefficient of the Stochastic OU Process:* This subsection shows the estimation accuracy of the proposed method under normal operating conditions by considering radically different autocorrelation coefficients of the OU stochastic process associated with the loads. As previously mentioned, the autocorrelation used during the rest of this work is 0.5 Hz, which, according to [33], is classified as a high-speed exponentially decaying autocorrelation and is within the range of real-life stochastic processes found in power systems. However, based on the composition of the loads and the electric network extension, the frequency fluctuations of the system may be represented by stochastic OU processes of quite different autocorrelation values. Thus, it is relevant to assess if the proposed estimator remains reliable under a wide variety of stochastic OU processes. To address this issue, an autocorrelation coefficient of 0.01 Hz (low-speed exponentially decaying autocorrelation [33]) is considered in this subsection, while the standard deviation remains equal to 1%. As before, a 6-hour long simulation with independent observation windows of different lengths is considered. As depicted in Fig. 5, the estimation accuracy with 5- and 3-minute-long observation windows has slightly degraded compared to the previous case study. The rationale behind this result is that the smaller the autocorrelation coefficient, the smaller the variability of the OU process, and thus the harder is for the iterative EE estimator to extract the inertia information since it works better with signals with high variations. However, this inconvenience can be easily compensated by using wider observation windows. For instance, as shown in Fig. 5, an 8-minute-long observation window allows for reliable estimations with small deviations around the mean value for all four areas of the IEEE 39-bus system.

Finally, to show that the proposed estimator is capable of detecting time-varying inertia with ambient measurements of

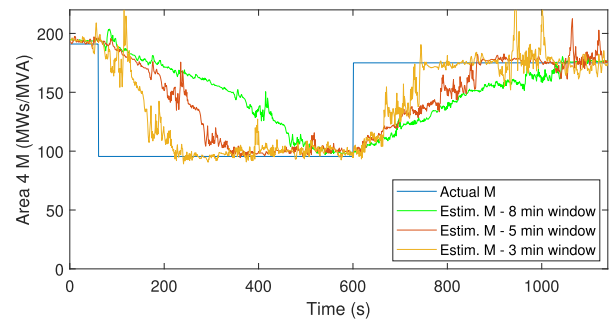


Fig. 6. IEEE 39-bus system—Time-varying M detected by ambient measurements (autocorrelation of 0.01 Hz).

different stochastic OU processes, the case of study presented in Section IV-A2 and in Fig. 4 is replicated with an autocorrelation value of the OU process of 0.01 Hz.

As can be seen in Fig. 6, with observation windows of different dimensions it is still possible to track the time-varying inertia value of areas. As in the previous study case, the wider the observation window, the more accurate the estimation but the slower the detection of the parameter change.

As shown in this subsection, the proposed method is able to carry out reliable inertia estimation considering ambient measurements characterized by a wide range of autocorrelation values. As mentioned earlier, this fact is particularly relevant since it shows that the proposed approach can be used in different types of electric networks.

4) *Power Imbalance Events:* The proposed methodology proves to be effective for the area inertia estimation also using ringdown signal measurements, i.e., after power imbalance events. Table II shows some power imbalance events of different magnitudes, and located at different buses of the network, simulated separately on the IEEE 39-bus test system. All the events occur at time $t = 1$ s and the observation window used to carry out the estimation is 30 s. The first four events refer to load outages, which imply a positive power imbalance for the system. The fifth and sixth events refer to power increases, therefore the power imbalance is negative. As reported in the last two rows, the methodology provides accurate estimations also following line outages. In fact, these kinds of events provoke oscillations throughout the network that can be used by the proposed algorithm to carry out the area inertia estimation. It

TABLE II
IEEE 39-BUS SYSTEM—M ESTIMATION ERRORS AFTER POWER IMBALANCE
EVENTS WITH GENERATOR CLUSTERING

	Area 1	Area 2	Area 3	Area 4
Load 16 outage (329 MW)	-0.4%	5.6%	-3.9%	-1.2%
Load 23 outage (248 MW)	-0.7%	4.4%	-2.9%	-1.3%
Load 8 outage (522 MW)	0.1%	-7.2%	-1.2%	-1.3%
Load 31 outage (9.2 MW)	1.8%	2.0%	2.9%	1.7%
Load 21 +50% (-137 MW)	0.2%	2.3%	-5.2%	-0.2%
Load 29 +10% (-28.4 MW)	3.5%	-1.2%	-0.5%	-3.0%
Line 4-5 outage	2.3%	-6.6%	-3.5%	-1.9%
Line 25-26 outage	2.0%	-1.9%	-1.9%	-4.5%

should be noted that also in this subsection the stochastic process of loads is considered.

By observing Table II it is possible to notice that, generally, the estimates are very accurate. However, there are some estimations that present slightly higher errors. For instance, the estimation of area 2 following load 8 outage presents a relative error of -7.2%. This error is caused by the fact that the event occurs in area 2, and the frequency measurements used to carry out the internal frequency estimations using the method proposed in [27] are affected by spikes and oscillations, particularly during the first instants after the perturbation. This, in turn, provokes slightly worse area inertia estimates. Similarly, it can be observed that the load 21 power increase provokes worse inertia estimates of area 3, and that the estimations of area 4 after the outage of line 25–26 are not as accurate as those related to other areas.

Finally, it is worth noticing that simulation results are obtained using the generator clustering algorithm. The threshold used by the clustering method is $3 \cdot 10^{-5}$ (p.u.) and has been determined empirically by carrying out a few clustering proofs. The RMS metric (21) is computed over the first 3 seconds after the power imbalance. In this network, which is characterized by having generators of the same area that are quite coherent in terms of electromechanical oscillations, the usage of the generator clustering algorithm is not essential. However, as shown in the next subsection, the benefit of using this clustering algorithm is more evident for grids lacking very coherent areas, such as the IEEE 118-bus system.

B. Test Results on the IEEE 118-Bus Test System

In this subsection, the accuracy of the proposed method in the IEEE 118-bus test system is reported. The interested reader can find the topological data and the power flow test case of the IEEE 118-bus network in [36]. Since the dynamic data of the network are not available in the literature, we take a guess on the type of power plant (e.g., hydroelectric, coal, gas, etc) connected to each bus based on the rated active power. Consequently, coherent governors, AVRs, and PSSs are selected in accordance with the power plant category.

The network has been modified by substituting SGs with CIGs at buses 49, 54, 59, 61, 65, 66, 80, 89, and 100. The system is divided into 4 areas: the first area comprises the SGs located in the western part of the network, namely the SGs connected to buses 10, 12, 25, 26, and 31; the second area includes SGs connected at buses 46, and 69, and the CIG at bus 80; area 3

TABLE III
IEEE-118 BUS SYSTEM—AREA COMPOSITION AND INERTIA VALUES

	Area 1	Area 2	Area 3	Area 4
Area composition	SGs 10/12/25 26/31	SGs 46/69 CIG 80	CIGs 49/54/59 61/65/66	SGs 87/103/111 CIGs 89/100
Equivalent transfer function	2 poles, 1 zero	2 poles 1 zero	1 pole	1 pole
SG-CIG M (MWs/MVA)	30.3/19/35.2 27.3/6.6	13.2/75/ 30	25/9/30 13/60/80	5.4//14/12.6/ 98/49
Area M (MWs/MVA)	118.4	118.2	217	179

is located in the northeast zone of the network and includes CIGs connected at buses 49, 54, 59, 61, 65, and 66; finally, area 4 includes generation units located in the southern part of the grid, namely SGs at buses 87, 103, and 111 and CIGs at buses 89, and 100. The composition of the areas, along with the inertia values of the single devices and of the areas, is summarized in Table III. As described in the previous subsection, these areas are identified empirically by grouping generators that are electrically near. Other compositions for areas 2 and 3 are possible since these zones are not clearly separated; simulations have shown that estimation results remain accurate with other area compositions.

An equivalent transfer function of the second order is used for area 1, which is composed only of SGs. Area 3 is composed only of CIGs, thus its equivalent transfer function is of the first order. Area 2 is composed of two SGs connected to buses 46 and 69, and one CIG connected to bus 80. In this area, the dominant generation unit is SG 69 due to its bigger apparent power (and inertia constant). Therefore, the used transfer function for the area has 2 poles and one zero. Area 4 presents 3 SGs connected at buses 87, 103, and 111, and 2 CIGs connected at buses 89, and 100. However, the effect of these two CIGs is dominant, due to their higher apparent power, and the equivalent transfer function of the area is of the first order. Regarding the selection of the transfer function order of mixed areas 2 and 3, similar considerations can be made with respect to the IEEE 39-bus network. The estimations obtained using different transfer function orders are strongly biased and can be therefore discarded by the TSO.

1) *Robustness to the Presence of Outliers:* Since PMU measurements may be affected by outliers, the robustness of the proposed method for this type of event is assessed. A 6-hour simulation using 5- and 3-minute-long observation windows is carried out. As in the previous case, the observation windows do not overlap in time, thus, 72 and 120 independent observation windows are considered, respectively. In each window, 100 outliers are inserted (corresponding to a simulation time of 1 s). Particularly, the electric frequency measurement of the bus connected to CIG 100 is supposed to remain frozen for 1 s due to a PMU malfunction. The inertia of area 4 is estimated considering the above outliers.

As we can observe in Table IV, the presence of bad data in the measurement set has a relatively limited effect since the increment of the mean error with respect to the case where no outliers are considered is negligible. This is expected since the proposed method uses observation windows of several minutes and thus, if the PMU fault occurs for a limited time, it does not carry significant weight over the final estimation accuracy.

TABLE IV
IEEE 118-BUS SYSTEM–M ESTIMATION AVERAGE ERRORS OF AREA 4
CONSIDERING MEASUREMENT OUTLIERS

	5 min observation window	3 min observation window
without outliers	2.95%	3.18%
with outliers	3.03%	3.36%

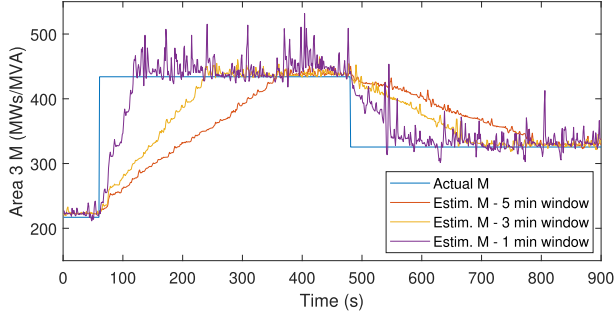


Fig. 7. IEEE 118-bus system–Time-varying M detected by ambient measurements.

Furthermore, since the area inertia estimation is carried out by grouping several generation unit measurements, the presence of bad data in one generation unit signal has a limited effect. As expected, the 5-minute long window is less affected than the 3-minute long window by the presence of the outliers since it is wider, and therefore the weight of the bad data over the time span covered by the window is smaller. However, more complex situations such as longer measurement faults or the presence of multiple interacting and conforming bad data that affect simultaneously several generation units (e.g., caused by a cyber-attack), should be carefully assessed. To deal with these issues, a robust version of the proposed iterative EE algorithm may be developed in the future.

2) *Time-Varying Inertia Under Normal Operating Conditions*: The capability of the proposed method to detect varying inertia of areas by using ambient measurements is tested also in this network. A simulation of 20 minutes is carried out. The generation units of area 3 double their inertia contribution at a simulation time of 6 minutes by acting on their control systems, thus increasing the inertia of the area to 434 MWs/MVA. This condition is maintained for 7 minutes, i.e., until the simulation time reaches 13 minutes. After that, all generation units reduce their inertia parameter by 25%, which corresponds to 325.5 MWs/MVA. As depicted in Fig. 7, the proposed method is capable of tracking the change of the inertia. As in the previous study case, wider observation windows provide more accurate estimates but slower updating times. This is due to the fact that they require more time for measurements related to previous inertia values to be left out by the moving window. The CPU time required by the proposed method to carry out one estimation with a 5-minute-long observation window is approximately 10 ms, which is well below the time offset of 1 s. Therefore, the algorithm can be applied online.

3) *Power Imbalance Events and Effect of the Generator Clustering Algorithm*: Table V reports the estimation errors of the proposed method using ringdown signals. It can be appreciated

TABLE V
IEEE 118-BUS SYSTEM–M ESTIMATION ERRORS AFTER POWER IMBALANCE
EVENTS WITH GENERATOR CLUSTERING

	Area 1	Area 2	Area 3	Area 4
Load 59 outage (277 MW)	1.0%	−3.3%	1.8%	−0.5%
Load 80 outage (130 MW)	−2.6%	0.0%	0.6%	1.1%
Load 82 outage (54 MW)	−3.1%	−0.1%	0.9%	3.1%
Load 1 outage (51 MW)	−0.5%	4.8%	2.3%	−1.2%
Load 118 outage (33 MW)	1.0%	−1.2%	1.7%	1.0%
Load 40 +50% (−66 MW)	1.5%	3.8%	2.7%	−2.9%
Load 60 +50% (−39 MW)	2.4%	−0.4%	2.0%	0.7%
Load 85 +50% (−15.8 MW)	1.7%	1.1%	1.4%	2.7%

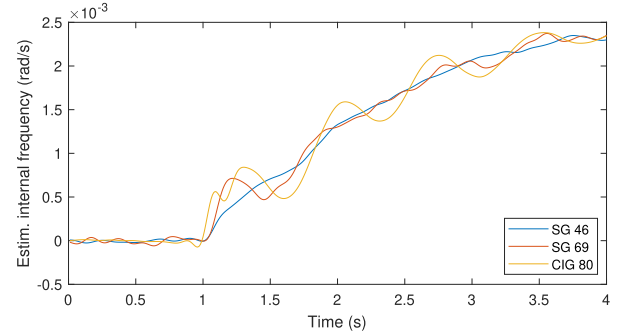


Fig. 8. IEEE 118-bus system–Internal frequency variations of area 2 after load 80 outage.

that the estimates are quite accurate, even for events that cause different power imbalances (ranging from a few MW to several hundreds of MW) and occur at different locations. These results confirm that the proposed methodology can estimate the inertia of areas also using ringdown signals.

In this network, generators grouped in the same area tend to oscillate differently when power imbalance events occur. Since the accuracy of the proposed method depends on the coherency of the generators in terms of electromechanical oscillations, it is important to separate non-coherent generators. Thus, in this study case, we focus on the effect of the proposed generator clustering algorithm on the area inertia estimations. It is worth mentioning that the threshold used in this network to group generators is $4.5 \cdot 10^{-5}$ (p.u.), which has been determined empirically. Also in this case, the RMS distance metric is computed during the first 3 seconds after the event.

The following is an example of the benefits that the clustering algorithm brought to the area inertia estimations. Fig. 8 represents the estimation of the internal frequency variations (using the model-independent estimator [27]) of the three generators of area 2 caused by the outage of load 80. It is possible to observe that they experience quite different oscillations. Therefore, it is not possible to group together their measurements for a joint estimation, since their electromechanical behavior can not be represented through a single transfer function. The clustering algorithm detects that the three generators have mutual distances higher than the threshold and separates them. At this point, the area inertia estimator carries out the estimation individually and it provides values of 13.5 MWs/MVA, 73.2 MWs/MVA, and 31.5 MWs/MVA, for the SG 46, SG 69, and CIG 80, respectively. These inertia values are then summed to get an

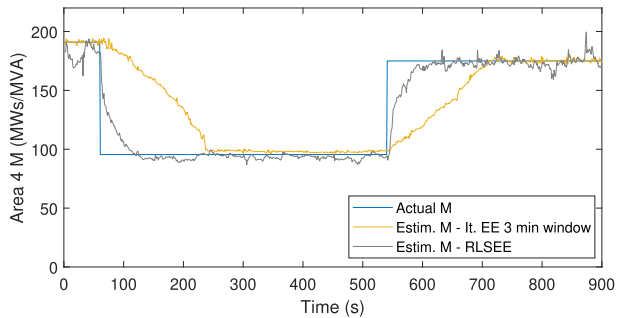


Fig. 9. IEEE 39–Time-varying M detected by ambient measurements (comparison with the RLSEE estimator).

area inertia value of 118.2 MWs/MVA, which equals the real inertia value. Without generator clustering, the estimation would provide a strongly biased estimation of 147.0 MWs/MVA for area 2, with a relative error of 24.3%. It is worth pointing out that the individual estimates of the three generators are quite accurate (see the inertia values of the single devices in Table III). Thus, the proposed estimator is very accurate also if applied to individual generation units.

C. Comparison With Other Estimators

This section compares the proposed method with other inertia estimation algorithms. A recently proposed recursive least-square equation error (RLSEE) [24] estimator is used to track time-varying inertia values of Section IV-A2, and the results of the two estimators are reported in Fig. 9. As expected, the RLSEE shows faster tracking capabilities since it does not use observation windows and the parameter update occurs recursively, i.e., every time a new measurement becomes available. However, this comes with the disadvantage of providing less accurate estimations since the weight of the measurement noise is higher for a recursive-based estimator than for an iterative-based one. Moreover, as detailed in [24], the RLSEE is applicable under normal operating conditions only by implementing a covariance matrix resetting, which is a non-trivial and scenario-dependent procedure.

Another recently-developed method uses convolutional neural networks (CNN) to estimate the power system momentum [37]. A CNN can accurately follow steps of momentum with a mean absolute percentage error of around 1%, which is comparable to what can be obtained with the method presented here. However, as with most machine-learning-based methods, this comes at the cost of a significantly large training dataset used for training the method and ensure adequate estimation capabilities (i.e., a low prediction error), which in general may not be easily available.

Table VI presents a comparison with other works in terms of estimation accuracy, applicability, and CPU times. The proposed estimator is one of the few methods capable of handling areas with a mixed composition of both SGs and CIGs. Besides, it is one of the few estimators applicable in real-time since the updating CPU times are sensibly smaller than the time offset of the sliding window. Furthermore, as far as we know, it is the

TABLE VI
COMPARISON WITH OTHER AREA INERTIA ESTIMATORS

Reference	Computational time (s)	Average estimation error		
		Normal operat. conditions	Power imbalance events	Applicability
[13]	$\approx 10^1$	Not applicable	$\approx 10 - 20\%$	Only SGs
[14]	Not reported	Not applicable	$\approx 5 - 15\%$	Only SGs
[15]	Not reported	Not applicable	$\approx 1\%$	Only SGs
[16]	$\approx 10^{-1}$	Not applicable	$\approx 3 - 5\%$	Mixed areas
[17]	Not reported	Not applicable	$\approx 4 - 5\%$	Only SGs
[18]	Not reported	Not applicable	$\approx 1 - 3\%$	Mixed areas
This work	$\approx 10^{-2}$	$\approx 2 - 4.5\%$	$\approx 1.5 - 3.5\%$	Mixed areas

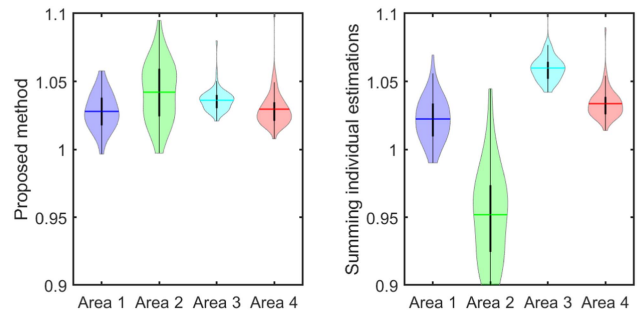


Fig. 10. IEEE 118-bus system– M normalized estimation with the proposed method (left) and summing individual estimations (right).

only area estimator capable of using both ambient and ringdown signal measurements.

D. Further Remarks

The proposed method can be used to compute the M value of single-generation units. Thus, one may come up with the idea of estimating the M of an area by summing the inertia of its generation units. Although this is a viable option, the estimations are more accurate if the input and output signals are merged as described in Section III. Indeed, by computing equivalent input and output signals of the areas, the effect of the measurement noise is reduced and area estimations are more precise and reliable. To support this claim with a numerical simulation, the IEEE 118-bus system was analyzed for 6 hours under normal operating conditions by using 72 independent 5-minute-long observation windows. The M estimation of the areas was performed using both the proposed approach and summing up the estimation of the individual generation units. As shown in Fig. 10, not only is the proposed method more precise as the mean value of the violin plots is closer to 1, but it also presents smaller deviations around the mean value. Thus, we advocate implementing the proposed approach by merging the input and output signals based on the information received by the generator clustering method.

The inertia estimations based on the electrical frequency measurements are generally very accurate. However, all the simulations shown in subsections IV-A and IV-B were carried out a second time using noisy tachometer measurements, supposing that these are available to the TSO (which may not be a realistic scenario). The usage of these measurements provides even more accurate results since the estimation process of the internal frequencies [27] intrinsically implies some imprecision. Therefore, for even better estimates, we advocate using tachometer measurements whenever they are available.

Finally, it is worth mentioning that, as the accuracy of system identification methods does not depend on the order of the transfer function of the device to be monitored, we do not predict any criticality in applying the proposed estimator to CIGs with other control schemes.

V. CONCLUSION

This article proposes an iterative EE SI approach to carry out the inertia estimation of areas, which provides accurate estimates using ambient measurements of different stochastic characteristics. Interestingly, the algorithm also shows good robustness to the presence of measurement outliers and the capability to track time-varying inertia by using a moving observation window. Furthermore, the proposed method is also capable of extracting information from ringdown signal measurements (power imbalance events). In this regard, a number of simulations on two test networks shows that the precision of the estimates is not particularly affected by the location and the magnitude of the power imbalance events. Indeed, unlike other works, neither of these two features needs to be known to carry out the estimation.

Future work may be devoted to the formulation of an equivalent area transfer function that does not simply cluster together generation units and includes several other factors such as loads and the topology of the area. So doing, the effective inertia seen from a particular point of the network should be provided. Another possible research line may be the development of a robust iterative EE SI method to handle multiple interacting and conforming outliers and missing data. Furthermore, in case the dynamics of an area with mixed composition are not accurately captured by an equivalent transfer function of integer order, the usage of fractional-order transfer functions may be investigated.

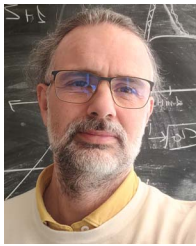
REFERENCES

- [1] F. Milano, F. Dorfler, G. Hug, D. J. Hill, and G. Verbič, "Foundations and challenges of low-inertia systems (Invited Paper)," in *Proc. Power Syst. Computation Conf.*, 2018, pp. 1–25.
- [2] ENTSO-E, "Technical group on high penetration of power electronic interfaced power sources, high penetration of power electronic interfaced power sources and the potential contribution of grid forming converters," Tech. Rep., 2020. [Online]. Available: https://eepublicdownloads.entsoe.eu/clean-documents/Publications/SOC/High_Penetration_of_Power_Electronic_Interfaced_Power_Sources_and_the_Potential_Contribution_of_Grid_Forming_Converters.pdf
- [3] E. Heylen, F. Teng, and G. Strbac, "Challenges and opportunities of inertia estimation and forecasting in low-inertia power systems," *Renewable Sustain. Energy Rev.*, vol. 147, Sep. 2021, Art. no. 111176.
- [4] B. Tan, J. Zhao, M. Netto, V. Krishnan, V. Terzija, and Y. Zhang, "Power system inertia estimation: Review of methods and the impacts of converter-interfaced generations," *Int. J. Elect. Power Energy Syst.*, vol. 134, Jan. 2022, Art. no. 107362.
- [5] K. Prabhakar, S. K. Jain, and P. K. Padhy, "Inertia estimation in modern power system: A comprehensive review," *Electric Power Syst. Res.*, vol. 211, Oct. 2022, Art. no. 108222.
- [6] A. Ortega and F. Milano, "A method for evaluating frequency regulation in an electrical grid - Part II: Applications to non-synchronous devices," *IEEE Trans. Power Syst.*, vol. 36, no. 1, pp. 194–203, Jan. 2021.
- [7] M. Liu, J. Chen, and F. Milano, "On-line inertia estimation for synchronous and non-synchronous devices," *IEEE Trans. Power Syst.*, vol. 36, no. 3, pp. 2693–2701, May 2021.
- [8] G. Frigo, P. A. Pegoraro, and S. Toscani, "Tracking power systems events: PMU, reporting rate, interpolation," in *Proc. Int. Conf. Smart Grid Synchronized Meas. Analytics*, 2022, pp. 1–6.
- [9] B. Tan, J. Zhao, V. Terzija, and Y. Zhang, "Decentralized data-driven estimation of generator rotor speed and inertia constant based on adaptive unscented Kalman filter," *Int. J. Elect. Power Energy Syst.*, vol. 137, May 2022, Art. no. 107853.
- [10] B. Tan and J. Zhao, "Data-driven time-varying inertia estimation of inverter-based resources," *IEEE Trans. Power Syst.*, vol. 38, no. 2, pp. 1795–1798, Mar. 2023.
- [11] F. Bizzarri, D. d. S. Giudice, S. Grillo, D. Linaro, A. Brambilla, and F. Milano, "Inertia estimation through covariance matrix," *IEEE Trans. Power Syst.*, vol. 39, no. 1, pp. 947–956, Jan. 2024.
- [12] J. Guo, X. Wang, and B. T. Ooi, "Estimation of inertia for synchronous and non-synchronous generators based on ambient measurements," *IEEE Trans. Power Syst.*, vol. 37, no. 5, pp. 3747–3757, Sep. 2022.
- [13] K. Tuttelberg, J. Kilter, D. Wilson, and K. Uhlen, "Estimation of power system inertia from ambient wide area measurements," *IEEE Trans. Power Syst.*, vol. 33, no. 6, pp. 7249–7257, Nov. 2018.
- [14] J. Schiffer, P. Aristidou, and R. Ortega, "Online estimation of power system inertia using dynamic regressor extension and mixing," *IEEE Trans. Power Syst.*, vol. 34, no. 6, pp. 4993–5001, Nov. 2019.
- [15] M. Sun, Y. Feng, P. Wall, S. Azizi, J. Yu, and V. Terzija, "On-line power system inertia calculation using wide area measurements," *Int. J. Elect. Power Energy Syst.*, vol. 109, pp. 325–331, Jul. 2019.
- [16] P. K. Dhara and Z. H. Rather, "Non-synchronous inertia estimation in a renewable energy integrated power system with reduced number of monitoring nodes," *IEEE Trans. Sustain. Energy*, vol. 14, no. 2, pp. 864–875, Apr. 2023.
- [17] B. Wang, D. Yang, G. Cai, Z. Chen, and J. Ma, "An improved electromechanical oscillation-based inertia estimation method," *IEEE Trans. Power Syst.*, vol. 37, no. 3, pp. 2479–2482, May 2022.
- [18] W. Zhong, G. Tzounas, M. Liu, and F. Milano, "On-line inertia estimation of virtual power plants," *Electric Power Syst. Res.*, vol. 212, Nov. 2022, Art. no. 108336.
- [19] L. Ljung, *System Identification: Theory for the User*, 2nd ed. London, U.K.: Pearson Education, 1998.
- [20] P. S. Diniz, *Adaptive Filtering: Algorithms and Practical Implementation*. New York, NY, USA: Springer, 2013.
- [21] P. Kundur, *Power System Stability and Control*. New York, NY, USA: McGraw-Hill, 1994.
- [22] K. Y. Yap, C. R. Sarimuthu, and J. M.-Y. Lim, "Virtual inertia-based inverters for mitigating frequency instability in grid-connected renewable energy system: A review," *Appl. Sci.*, vol. 9, no. 24, 2019, Art. no. 5300. [Online]. Available: <https://www.mdpi.com/2076-3417/9/24/5300>
- [23] M. S. K. Deergha Rao, *Digital Signal Processing: Theory and Practice*. Singapore: Springer, 2018.
- [24] D. Gotti, P. Ledesma, and H. Amaris, "A recursive system identification inertia estimator for traditional and converter-interfaced generators," *Int. J. Elect. Power Energy Syst.*, vol. 154, 2023, Art. no. 109445. [Online]. Available: <https://www.sciencedirect.com/science/article/pii/S0142061523005021>
- [25] A. S. Cheam and M. Fredette, "On the importance of similarity characteristics of curve clustering and its applications," *Pattern Recognit. Lett.*, vol. 135, pp. 360–367, Jul. 2020.
- [26] S. Shalev-Shwartz and S. Ben-David, *Understanding Machine Learning: From Theory to Algorithms*. Cambridge, U.K.: Cambridge Univ. Press, 2014.
- [27] F. Milano, A. Ortega, and A. J. Conejo, "Model-agnostic linear estimation of generator rotor speeds based on phasor measurement units," *IEEE Trans. Power Syst.*, vol. 33, no. 6, pp. 7258–7268, Nov. 2018.
- [28] D. Gotti, "Dynamic data of generation units of the IEEE 39- and 118-bus test systems and powerfactory files," 2023, doi: [10.13140/RG.2.2.26903.75680](https://doi.org/10.13140/RG.2.2.26903.75680).
- [29] B. Barac, M. Krpan, T. Capuder, and I. Kuzle, "Modeling and initialization of a virtual synchronous machine for power system fundamental frequency simulations," *IEEE Access*, vol. 9, pp. 160116–160134, 2021.
- [30] F. Milano and R. Zafate-Miñano, "A systematic method to model power systems as stochastic differential algebraic equations," *IEEE Trans. Power Syst.*, vol. 28, no. 4, pp. 4537–4544, Nov. 2013.
- [31] M. Perninge, M. Amelin, and V. Knazkins, "Load modeling using the Ornstein-Uhlenbeck process," in *Proc. IEEE 2nd Int. Power Energy Conf.*, 2008, pp. 819–821.
- [32] M. Adeen and F. Milano, "Modeling of correlated stochastic processes for the transient stability analysis of power systems," *IEEE Trans. Power Syst.*, vol. 36, no. 5, pp. 4445–4456, Sep. 2021.
- [33] M. Adeen and F. Milano, "On the impact of auto-correlation of stochastic processes on the transient behavior of power systems," *IEEE Trans. Power Syst.*, vol. 36, no. 5, pp. 4832–4835, Sep. 2021.

- [34] R. H. Hirpara and S. N. Sharma, "An Ornstein-Uhlenbeck process-driven power system dynamics," *IFAC-PapersOnLine*, vol. 48, no. 30, pp. 409–414, 2015. [Online]. Available: <https://www.sciencedirect.com/science/article/pii/S2405896315030554>
- [35] M. Brown, M. Biswal, S. Brahma, S. J. Ranade, and H. Cao, "Characterizing and quantifying noise in PMU data," in *Proc. IEEE Power Energy Soc. Gen. Meeting*, 2016, pp. 1–5.
- [36] R. Christie, "118 bus power flow test case," 2023. [Online]. Available: https://labs.ece.uw.edu/pstca/pf118/pg_tca118bus.htm
- [37] D. Linaro et al., "Continuous estimation of power system inertia using convolutional neural networks," *Nature Commun.*, vol. 14, no. 1, 2023, Art. no. 4440.



Davide Gotti (Member, IEEE) received the M.Sc. degree in electrical engineering from Politecnico di Milano, Milano, Italy, in 2014, the M.Sc. degree in renewable energy in electrical systems, and the Ph.D. degree in electrical engineering from Universidad Carlos III de Madrid, Madrid, Spain, in 2018 and 2023, respectively. He has several years of experience in the renewable energy industry carrying out, among other activities, the design, model validation, and interconnection studies of photovoltaic power plants. His research interests include power system dynamic state estimation, electric network modeling, control, and stability analysis.



Federico Bizzarri (Senior Member, IEEE) was born in Genoa, Italy, in 1974. He received the Laurea (M.Sc.) five-year degree (*summa cum laude*) in electronic engineering and the Ph.D. degree in electrical engineering from the University of Genoa, Genoa, Italy, in 1998 and 2001, respectively. Since October 2018, he has been an Associate Professor with the Electronic and Information Department, Politecnico di Milano, Milan, Italy. He is a Research Fellow of the Advanced Research Center on Electronic Systems for Information and Communication Technologies "E.

De Castro" (ARCES), University of Bologna, Bologna, Italy.



Angelo Brambilla (Senior Member, IEEE) received the Dr.Ing. degree in electronics engineering from the University of Pavia, Pavia, Italy, in 1986. He is currently a Full Professor with the Dipartimento di Elettronica, Informazione e Bioingegneria, Politecnico di Milano, Milano, Italy, where he has been working in the areas of circuit analysis, simulation and modeling.



Davide del Giudice (Senior Member, IEEE) was born in Milan, Italy, in 1993. He received the M.S. and Ph.D. degrees in electrical engineering from the Polytechnic of Milan, Milan, Italy, in 2017 and 2022, respectively. He is currently a Researcher with the Department of Electronics, Information and Bioengineering, Polytechnic of Milan. His main research interests include simulation techniques for electric power systems with a high penetration of converter-interfaced elements, such as high voltage direct current systems, electric vehicles, and generation fuelled

by renewables.



Samuele Grillo (Senior Member, IEEE) received the Laurea degree in electronic engineering, and the Ph.D. degree in power systems from the University of Genova, Genova, Italy, in 2004 and 2008, respectively. He is currently an Associate Professor with the Dipartimento di Elettronica, Informazione e Bioingegneria, Politecnico di Milano, Milan, Italy. Since 2018, he has been a Contributor to CIGRÉ Working Group B5.65 "Enhancing Protection System Performance by Optimising the Response of Inverter-Based Sources." His research interests include smart

grids, integration of distributed renewable sources, and energy storage devices in power networks, optimization, and control techniques applied to power systems.



realistic single-cell models of neuronal cells.

Daniele Linaro (Member, IEEE) received the M.Sc. degree in electronic engineering and the Ph.D. degree in electrical engineering from the University of Genoa, Genoa, Italy, in 2007 and 2011, respectively. Since 2018, he has been an Assistant Professor with the Department of Electronics, Information Technology and Bioengineering, Polytechnic of Milan, Milan, Italy. His research interests include circuit theory and nonlinear dynamical systems, with applications to power systems, electronic oscillators, and computational neuroscience, in particular biophysically-

Pablo Ledesma Larrea received the Ph.D. degree with the University Carlos III of Madrid, Spain. He is currently an Associate Professor with the University Carlos III of Madrid. He was with the Spanish TSO on several projects on large-scale integration of renewable energy. He has been an Academic Visitor with Chalmers University, Gothenburg, Sweden and Strathclyde University, Glasgow, U.K. His research interests include transient stability and dynamic modeling of power systems.

Hortensia Amaris (Senior Member, IEEE) received the Electrical Engineer and the Ph.D. degrees from the Technical University of Madrid (UPM), Madrid, Spain, in 1990 and 1995, respectively. She is currently a Full Professor of electrical engineering with the University Carlos III of Madrid, Madrid, Spain, where she has been working mainly on operation and control of power networks, power quality, power-electronic converters, renewable energy sources, and smart grids.